ACS APPLIED MATERIALS & INTERFACES

www.acsami.org

Research Article

Dual-Ionomer-Based Device: Acetylcholine Transport and Nonenzymatic Sensing

Nazrin Abdullayeva, Alihan Kumtepe, Cigdem Tuc Altaf, Hakan Seckin, Nurdan Demirci Sankir,* and Mehmet Sankir*

Cite This: https://dx.doi.org/10.1021/acsami.0c13725

Read Online

ACCESS | Metrics & More | Article Recommendations | Supporting Information

ABSTRACT: The malfunctioning in the release of acetylcholine (ACh^+), leading to consequential damages in the neural system, has become an impulsion for the development of numerous progressive transport and detection gadgets. However, several challenges, such as laterality and complexity of transport devices, low precision of amperometric detection systems, and sumptuous, multistaged enzymatic quantification methods, have not yet been overcome. Herein, ionomers, because of their selective ion transporting nature, are chosen as suitable candidates for being implemented into both targeted ACh^+ delivery and sensing systems. Based on these two approaches, for the very first time in the literature, the disulfonated poly(arylene ether sulfone) membrane is concurrently (i) used in the mimicry of transduction of the electrical-to-ionic signal in a neural network as "Acetylcholine Pen" (ACh^+ Pen) and (ii) operated as a highly sensitive, conductivity-based ACh^+ quantifier. Our dual device, being able to operate under an actual action potential of 55 mV_{bias}, shows a strong potential of future applicability in real-time ionic delivery-and-sensing systems.

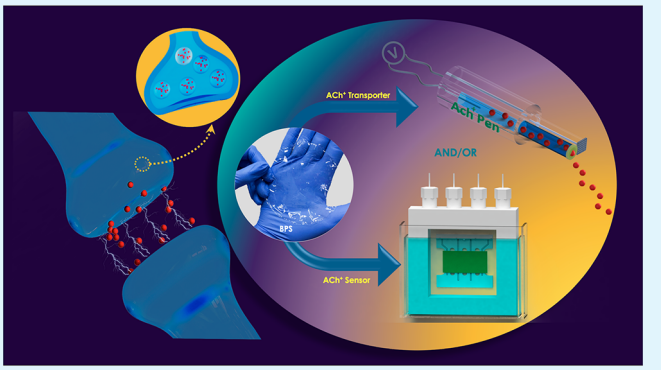

KEYWORDS: *ionomer, acetylcholine transport, biosensor, impedance spectroscopy, membrane*

1. INTRODUCTION

The inception of life on earth has been triggered by membranes. Membranes are the eternal artifacts of biosystems that have induced the nascence and persistence of vita.[1] The amphipathic bilayers of membranes constitute the protective layer that surrounds the living cells and has an essential selective mechanism that allows only the vital molecules in and out.[1,2] This selective mechanism attained in all living systems elucidates the importance of membranes in our habitat. Composing the fundamental role in living cells, membranes have found their implementation in artificial forms as well. For decades, membranes have been synthesized for various purposes and have been utilized in different application fields.[3−5] Within years, membranes came into use in the biotechnological field, where mimicry of the natural environments has been tried to be achieved.[6−9] Neural communication that is within our point of interest, in this study, is one of the major fields in which the implementation of ion-exchange membranes has been attempted.

The communication network within the neural microenvironment, which is responsible for the operability of biological systems, is highly complex.[10] The response obtained in the form of "neural cell activity" is both a spatial and a temporal context, which is also dependent on the nature of ions that create the communication signal. Neurotransmitters are the molecules responsible for the generation of cell-to-cell communication signals in-between neurons.[11] The malfunctioning in neurotransmitter transport mechanism or, in particular, the release of neurotransmitters at undesired amounts leads to a large variety of physiological disorders, among which Parkinson's disease, Alzheimer's disease, and epilepsy are the most widely encountered ones.[12−14] Acetylcholine (ACh^+), being one of the major representatives of the neurotransmitter family, is responsible for the signaling between skeletal muscles and motor nerves.[15] Their level in neural cells is regulated via choline acetyltransferase enzyme, and its presence in low amounts is the major cause of Alzheimer's disease.[16] To gain an insight into proper neural functioning, understanding the fundamentals of the signaling process and the action of the release of neurotransmitters is of extreme importance.

Received: July 30, 2020
Accepted: October 8, 2020

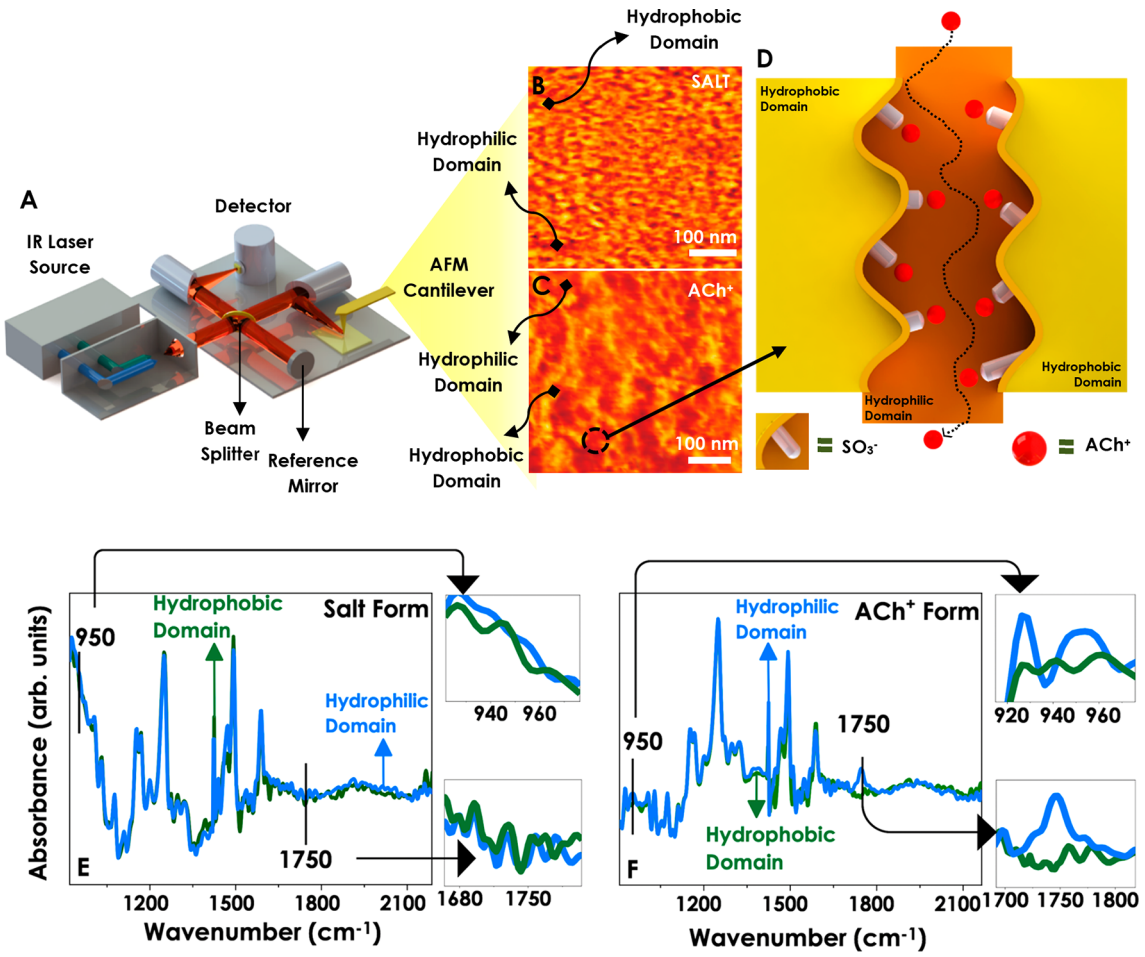

Figure 1. (A) Schematic representation of Nano-FTIR setup and 500 × 500 nm^2 AFM images obtained from (B) salt and (C) ACh^+ forms of membranes. (D) Mechanism responsible for the transport of ACh^+ through hydrophilic membrane domains. IR spectra obtained from (E) salt and (F) ACh^+ forms of membranes.

Iontronics and organic mixed ionic−electronic conductors (OMIECs) comprising the new generation of devices with the excellent temporospatial resolution are known as organic electronic systems that provide ionic or ionic−electronic transport through electrophoretic motion.[17,18] The operation principle of these appliances is based on conjugated polymers that possess both electrical and ionic conductivity, which provides the conversion of electronic pulses into ionic signals.[10,19−21] Despite many advantages of iontronic devices, some of which have excellent precision in spatiotemporal ionic delivery and have an unlimited supply of the transported ions, poor control maintained over the released amounts and rates hinders their preferability. Additionally, low ion transport rates, geometrical constraints, lateral design, and the requirement for higher bias voltages are among the main issues that need to be considered for further system improvement studies.

The incorporation of ion exchange membranes (IEM) into neural transport systems led the way to a new era of iontronics where, under applied bias, the non-flow-related electrophoretic motion of ions through the membrane to the target is the only determinant transport mechanism.[22,23] The most significant study based on IEM-related ionotronic transport devices has been recently reported by Poxson et al.[22] The study aimed to optimize the OEIP parameters to provide the transport of macromolecules such as aromatic and cyclic alkanes by using a hyperbranched polymer. However, for the given OEIP system, the crossover through the membrane to per-contra solution still took place in the lateral direction.

Being inspired by the evolutionary nature of membranes, herein, we report a dual system of ionomer-based acetylcholine (ACh^+) transporter and nonenzymatic sensor, holding a strong potential of becoming a pioneering membrane-based device that is going to treat neurotransmitter-related illnesses in the near future. The operability of both devices relies on disulfonated poly(arylene ether sulfone) (BPS) ionomer membrane which plays the role of ACh^+ transporter in potentiostatic systems and sensors in impedance measurements.[24−28] So far, BPS membranes have been used in various applications such as proton-exchange membrane fuel cells (PEMFCs), redox flow batteries, and desalination processes.[24−26,29,30] This material has been reported to exceed Nafion in both performance-based and economic aspects. Its facile synthesis and ability to be modified with the incorporation of certain pendant groups and blending with other copolymers is an advantageous feature allowing application-based optimizations of BPS.[31] Being thoroughly studied within our research group, the investigations of BPS and careful elaboration of its material properties have been reported in our previously published articles.[25,32] In this study, these BPS copolymers have been treated with ACh^+ salt solution and therefore subjected to a cationic exchange, which resulted in selective transportation of ACh^+. As a result, a novel

https://dx.doi.org/10.1021/acsami.0c13725
ACS Appl. Mater. Interfaces XXXX, XXX, XXX−XXX

device called "Acetylcholine Pen" (ACh^+ Pen), being the denotation used for ACh^+ transporter, which is a simple yet efficient system composed of a biocompatible BPS ionomer engaged to the tip of a pen filled with aqueous ACh^+ solution, has been introduced for the very first time in the literature.

BPS-based nonenzymatic sensor, on the other hand, possesses a smartly constructed, highly straightforward system design, where the membrane is being integrated into conductivity cell for the quantification of the amount of analyzed sample with unknown ACh^+ concentration. To the best of our knowledge, a neurotransmitter or, more specifically, ACh^+ sensors developed so far have been mostly enzyme-based systems conducting detection via enzymatic reaction cycles.[33−36] Nonetheless, the literature reports lack the presence of ionomer-based, straightforward, nonenzymatic sensing techniques that do not require long and consecutive preparation steps and have fast measurement times. The system developed here possesses several important novelties, among which (i) simple and scalable system design, (ii) successful ionic transportation under low voltages (55 mV), and (iii) nonenzymatic, single-staged ACh^+ sensing via the (iv) utilization of membrane's conductivity to transform the data into the concentration can be listed as the most significant ones. Besides, the combination of both BPS-based devices into a dual system enables the simultaneous actualization of ACh^+ transport and quantification. The realization of these two applications via a simple BPS ionomer is a technologically intriguing case, possessing a strong potential to be a new ground-breaking contribution to the literature.

2. RESULTS AND DISCUSSION

2.1. Acetylcholination of BPS and Basic Membrane Characterizations. BPS membranes being primarily synthesized in their salt forms have been consecutively protonated and acetylcholinated, as described in the Experimental Section. These experimental steps have been conducted to equilibrate the membrane channels for desired cationic transport. The ion-exchange capacity (IEC) values for protonated and acetylcholinated forms of membranes have been evaluated as 1.52 and 1.42 mequiv mg^{-1}, respectively, and explained in detail in the Experimental Section. Zeta-potential analyses have been performed on ACh^+ and H^+ forms of BPS, and the elaboration of experimental conditions is reported in the Experimental Section. Figure S1 gives the time-dependent zeta-potential distribution obtained from both membranes within 17 min of the analyses period, showing comparable results for ACh^+ and H^+ forms with average zeta-potentials being −15.7 and −16.4 mV, respectively. It is important to note that zeta-potential data are consistent with IEC values, where the results obtained for both forms of BPS are also in good proximity to each other. Several research groups have previously established that ionic conductivity in solid-state polymers actualizes as a result of randomized bouncing of ions in-between available counter-ionic groups.[27,29,30,37,38] Parameters like the size of ions and ease of dissociation of the target ion from the counterionic group are considered to be defining factors in the transport process.[37,39,40] Therefore, the detection of changes occurring as a result of polymer−ACh^+ interaction has been conducted via several characterization techniques. On the basis of the chemical structure of BPS that is given in Figure S2A, it is apparent that the sulfone groups of copolymers provide the interaction with ACh^+ ions. The visualization of changes in channels providing ionic crossover has been demonstrated via Nano-FTIR analysis, which has been chosen as a proper and precise characterization (Figure 1A).[41] The AFM phase images of Nano-FTIR have been obtained in tapping mode under ambient conditions. In the conducted analysis, the contrast has been established between salt form or, in other words, pristine and acetylcholinated form of BPS (ACh^+-BPS), and the acquired AFM phase images are given in Figure 1B,C. A distinct variation has been exhibited between the phase distributions of two different types of membranes. It has been observed that the overall chromatic dispersion of AFM images ranges within dark orange and light yellow regions, each individually representing hydrophilic and hydrophobic domains, respectively. The relatively dark orange hydrophilic domains appear to be softer due to the presence of water in sulfonic acid groups. In contrast, the light yellow color stands for the shrunk regions not containing sulfone groups and therefore not participating in ion transport processes.[30,42−45] It can be clearly seen that in a 500 × 500 nm^2 image the amount of stiff hydrophobic channels of salt form exceeds that of ACh^+-BPS. Moreover, a severe difference can be emphasized between the sizes of nanoscaled hydrophilic domains, confirming the eventual ACh^+ interaction. Figure 1D has been given to elucidate the concept of ionic transport through hydrophilic membrane channels. In the case of ACh^+ crossover through the membrane, the dielectric effect is assumed to be the dominating mechanism responsible for transport.[46] The interaction between two counterions results in the bouncing of ACh^+ ions among the anionic SO_3^- groups, which are present only within hydrophilic domains, thus providing the transport.

Expanding on the IR results obtained precisely from the membrane domains, Figures 1E and 1F show the spectrum obtained from both salt and ACh^+ forms of BPS, respectively. To provide a comprehensible comparison, IR sampling points have been indicated on the AFM images, and individual analogy has been established between hydrophilic and hydrophobic domains of both types of membranes. Figure 1E, giving a detailed IR spectrum comparison between light yellow and dark orange domains of pristine BPS, shows that no severe changes can be detected between hydrophilic and hydrophobic phases of salt form. On the other hand, ACh^+-BPS points out the presence of a highly significant difference between the two phases. As can be seen in zoomed regions of Figure 1F, a characteristic ACh^+ peak at ∼950 cm^{-1} has been detected for the hydrophilic domain, while no trace of the given molecular interaction has been encountered inside the hydrophobic phase. A similar case can be seen for higher wavenumbers, where a characteristic ACh^+ peak appearing at 1750 cm^{-1} has been observed to vanish while analyzing the hydrophobic domains of the exactly same membrane. Figures S2B and S2C have been given to emphasize the fact that the presence of characteristic ACh^+ peaks has only been encountered exactly within the hydrophilic channels and has not been detected in either hydrophobic domains or salt form of BPS. This characterization has been conducted as a strong assertion of the presence of interaction between ACh^+ and sulfone groups of membranes, therefore evidencing the means of ionic transport through its channels. In addition to Nano-FTIR spectroscopy, standard AFM of membranes have also been conducted. Similar to the results obtained from Nano-FTIR, a significant increase in hydrophilic domains has been observed for the polymers transferring gradually from salt to proton and then to acetylcholine forms (Figure S2D).

https://dx.doi.org/10.1021/acsami.0c13725
ACS Appl. Mater. Interfaces XXXX, XXX, XXX−XXX

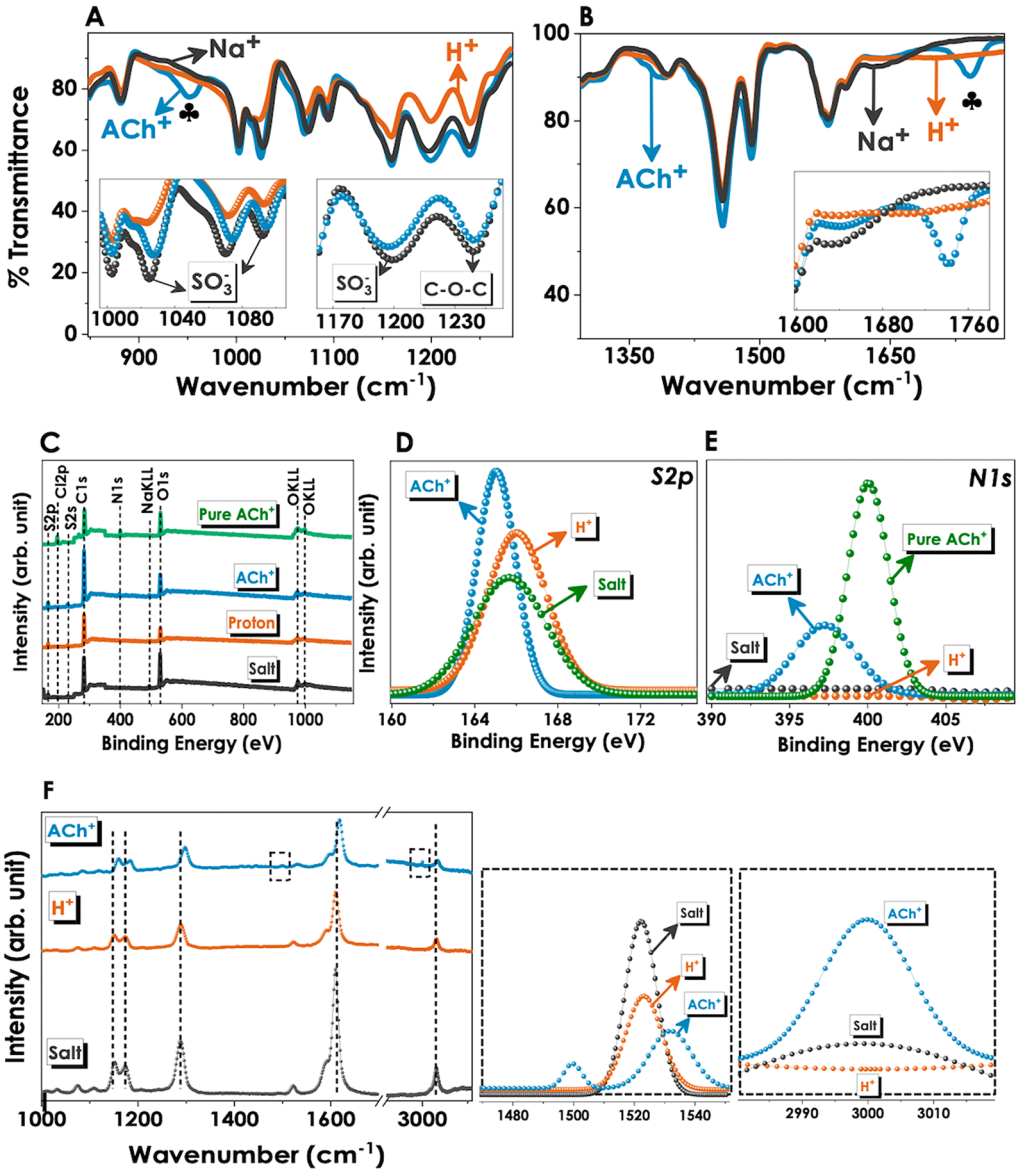

Figure 2. FTIR spectra of BPS in three different cationic forms analyzed at (A) 850−1300 cm^{-1} and (B) 1300−1800 cm^{-1} wavenumbers with inset figures focusing on distinct positional fluctuations. (C) XPS survey obtained from three different forms of BPS and pure acetylcholine chloride molecule with individual comparisons of (D) S 2p and (E) N 1s peaks. (F) Raman spectra of membranes with focused ACh^+ originated distinct peaks.

The presence of interaction between BPS and ACh^+ has been thoroughly traced back via FTIR spectroscopy (Figure S3A). Figures 2A and 2B zoom into the specific regions of the overall spectrum to point out the changes after different types of cationic loadings. Significant shifts have been observed at 1027, 1094, and 1204 cm^{-1} (inset Figure 2A) from which the first peak is assigned for the symmetric stretching of SO_3^- while the last two represent asymmetric stretching of SO_3^- groups.[42,47] Previous studies reported by Mauritz et al. and Kunimatsu et al. have investigated the changes in IR responses as a result of ion-exchange membrane hydration/dehydration and have stated that the presence of both peak shift and decrease in full width at half-maximum (FWHM) is directly related to the increase in water content of membrane.[48,49] Taking into consideration (i) the swelling in hydrophilic domain sizes after acetylcholination step, (ii) the presence of peak shifts, and (iii) the evidenced decrease in FWHM (Table S1), it can be concluded that the successful introduction of ACh^+ into hydrophilic BPS domains has been achieved. In addition, the appearance of non-BPS originated peaks marked as "♣" at 950 and 1750 cm^{-1} after acetylcholination steps has approved the change in ionic content of BPS signifying the characteristic $(N-CH_3)_3$ asymmetric stretching and C═O stretching, respectively (Figure S3B).

XPS analyses have been conducted on all three forms of membranes together with the pure acetylcholine chloride molecule for legitimate comparison purposes. Analyzing the overall XPS survey given in Figure 2C, oxygen, carbon, sulfur, and nitrogen elements have been chosen for individual analogy. All separate element examinations show a distinguishable presence of peak shifts after protonation and acetylcholination, proving that the chemical and electronic environment of membranes undergoes certain changes. Although O 1s, O KLL, and C 1s peaks, generated from two abundant elements that constitute the overall membrane molecular structure, show a positional variation in binding energy levels, it is highly

https://dx.doi.org/10.1021/acsami.0c13725
ACS Appl. Mater. Interfaces XXXX, XXX, XXX−XXX

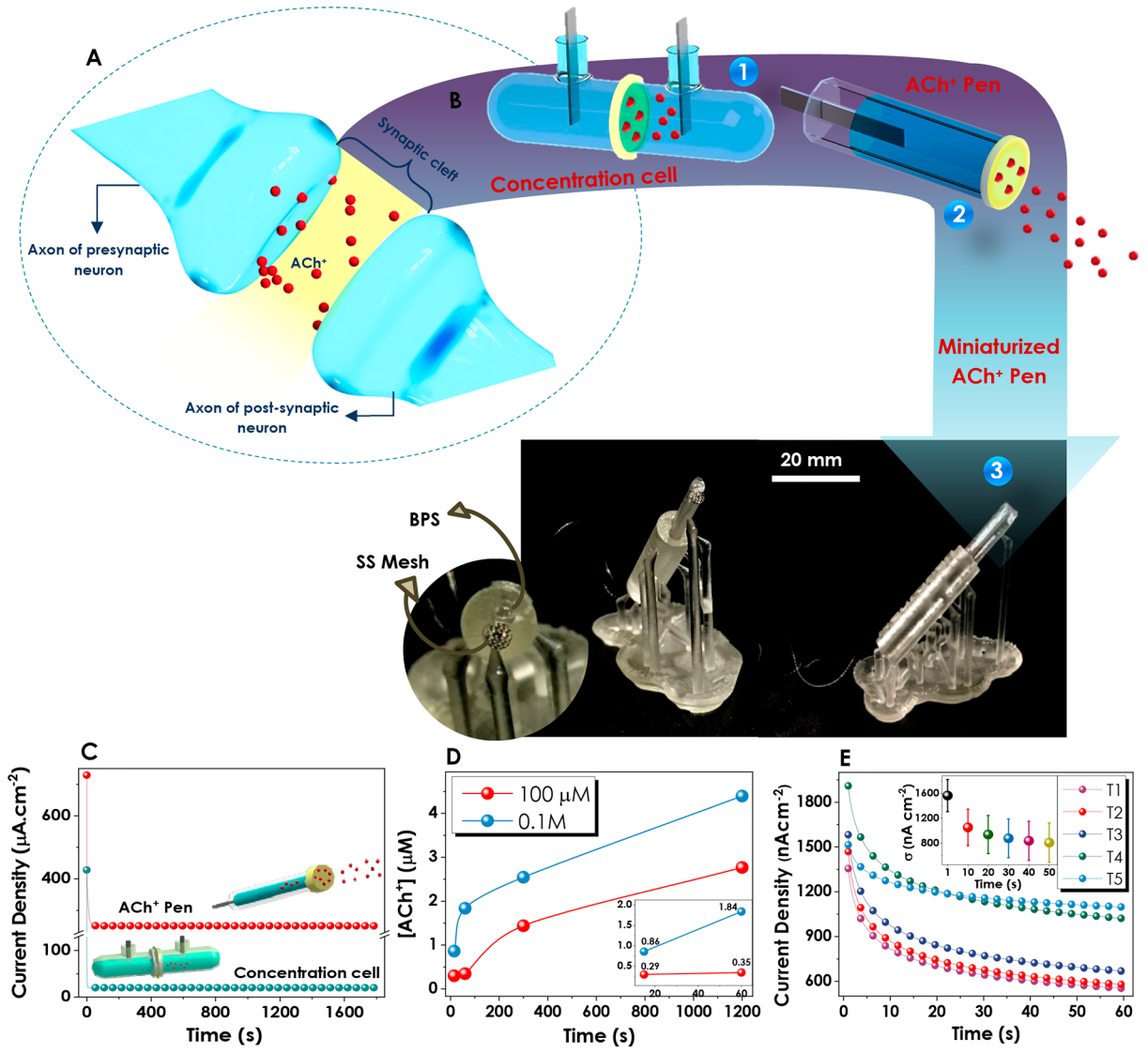

Figure 3. (A) Axonal transport through the synaptic cleft and correlation of ionic crossover mechanism with our systems. (B) Illustration of membrane-based self-designed transport devices at three different dimensions: (1) concentration cell, (2) ACh^+ Pen, and (3) miniaturized ACh^+ Pen (C) Current density vs time data obtained from concentration cell and ACh^+ Pen under 1 V_{bias}. (D) Fluorometric data obtained from ACh^+ Pen under 1 V_{bias} to testify/quantify the actualization of transport. (E) Potentiostatic analyses conducted on miniaturized ACh^+ Pen under 55 mV_{bias}.

complicated to interpret the origin of their shifts (Figure S3C–E). On the other hand, S 2p and N 1s peaks can be used as practical guides for understanding the origin of BPS and ACh^+ interaction. Upon analysis of Figure 2D, the S 2p peak shifts toward lower binding energy levels in the acetylcholinated form of BPS (ACh^+-BPS). Because the binding energy of a specific element is directly related to its chemical environment, a shift in an XPS peak can be associated with the changing electronegativity around the element of interest, sulfur. Considering that as a result of the interaction of $-SO_3^-$ of BPS with ACh^+'s N-$(CH_3)_3$, more electronegative oxygen is going to attract the electron cloud around nitrogen, thus increasing the surrounding electron density of the sulfone group. This increase in electron density is expected to result in a decrease in binding energy levels, which can be witnessed from the obtained XPS spectra.[50,51] The interpretation of N 1s peak is less complicated due to the absence of any nitrogen atom within the structure of BPS. Examining Figure 2E, it can be observed that any traces of N 1s have not been encountered in either salt or proton forms of BPS. On the contrary, a very significant peak appears in ACh^+-BPS, which is shifted compared to the N 1s peak of pure acetylcholine chloride. Raman analyses have served for the similar purpose of validation of the polymer–neurotransmitter interaction where the obtained spectra have revealed characteristic membrane peaks at 3080, 1610, 1288, 1175, and 1150 cm^{-1} (Figure 2F). Positional shifts have been observed for all of the mentioned characteristic peaks, among which 1610 cm^{-1} is assigned to the sulfonyl group conjugated benzene ring, 1175 cm^{-1} stands for O═S═O scissoring, and the rest of the peaks represent fundamental benzene ring generated vibrations.[52] The presence of weak, unprecedented peaks in ACh^+ form of the membrane is found to be originated from asymmetric deformation and symmetric stretching of CH_3 groups coupled to N–$(CH_3)_3$ of acetylcholine chloride (AChCl) at approximately 1500 and 3005 cm^{-1} wavenumbers, respectively.

2.2. BPS-Based Dual ACh^+ Transporter (ACh^+ Pen) and Sensor. *Part 1: ACh^+ Pen.* In the sequel of successful

https://dx.doi.org/10.1021/acsami.0c13725
ACS Appl. Mater. Interfaces XXXX, XXX, XXX–XXX

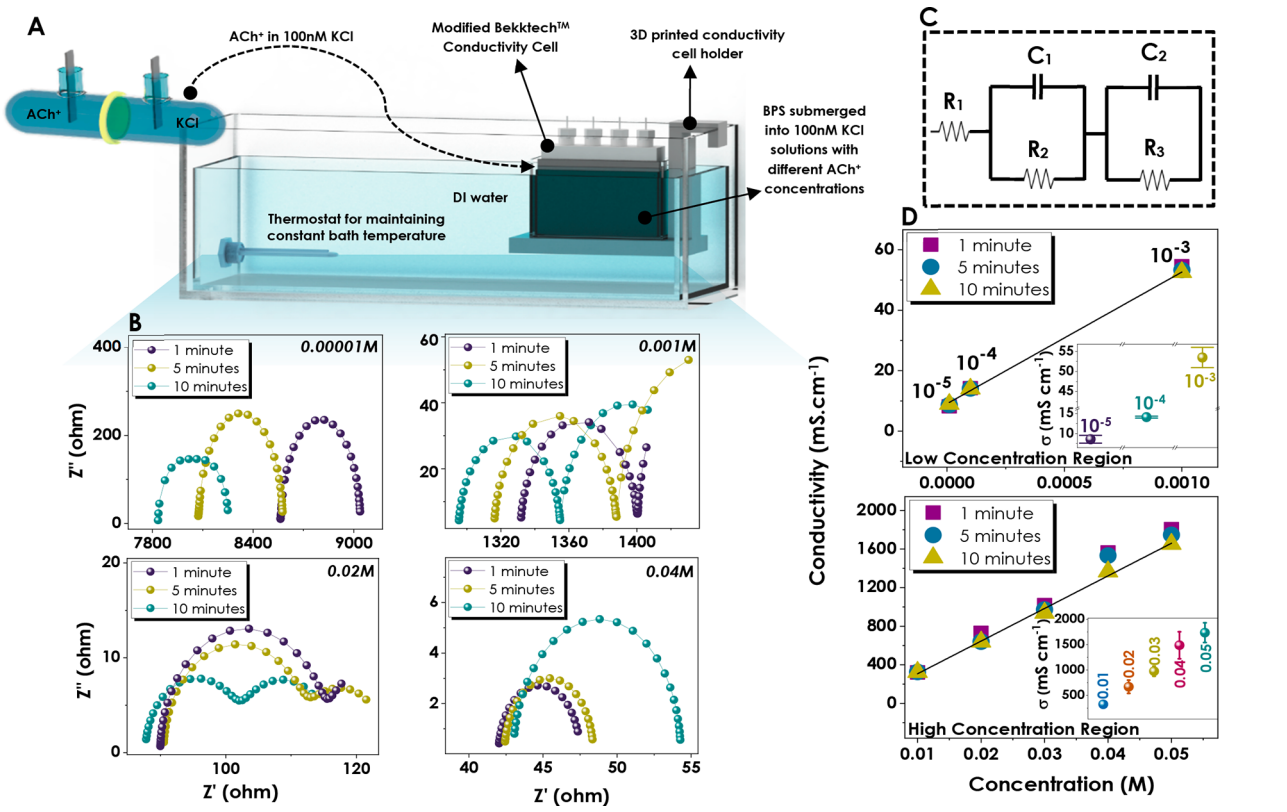

Figure 4. (A) Experimental setup for tandem system operation. (B) Equilibration of BPS at solutions containing different ACh^+ concentrations and standard 100 nM KCl. (C) EC used for impedance plot fittings. (D) Calibration curve of BPS conductivities in low and high ACh^+ concentration regions with corresponding error bars.

membrane preparation and characterization steps, the ready-to-use ACh^+-BPS has been implemented into a potentiostatic ion transport device. The system has been designed in a manner that mimics the axonal transport at nerve endings through the transportation of ACh^+ neurotransmitters from a synaptic cleft via electrophoretic motion (Figure 3A). Because the basis of neural communication underlies behind the consecutive electrical−chemical−electrical signal transductions, in the given system, ACh^+-BPS is the main component that provides the transport of particularly ACh^+ across its hydrophilic channels, creating a resistive barrier for the electrons and thus acting as the synaptic cleft. The proposed device architecture, named ACh^+ Pen, has been primarily designed at large scales, in a concentration cell composed of two compartments containing AChCl and potassium chloride (KCl) solutions at 0.1 M concentrations (Figure 3B-1). The operability of the concentration cell system has been analyzed via the potentiostatic technique under 1 V_{bias} where the stabilization of the generated current occurred within the primary 10 s, and an approximately constant value of 200 μA has been obtained throughout the 1800 s of transport duration (Figure S4A). After the crosscheck of the system operability at large dimensions, the diminution of the concentration cell into pen structures has been materialized. As a result, an ordinary pen with a membrane engaged on its tip served as the new device, ACh^+Pen, for the realization of ACh^+ transport (Figure 3B-2). The potentiostatic response obtained from ACh^+ Pen shows a slightly slower stabilization of current (Figure S4A), reaching a constant value of 70 μA within 32 s. The results obtained from potentiostatic experiments have been normalized to the cross-sectional area of membranes (8.6 cm^2 for large and 0.28 cm^2 for ACh^+ Pen scales) and are given in Figure 3C.

Although potentiostatic measurements served as successful methods for the testification of device operability, the quantification of the amount of transported ACh^+ from ACh^+ Pen has been done via the fluorometric technique, details of which are specified in the Experimental Section. The amounts of transported ACh^+ obtained from fluorometric analyses given in Figure 3D show that in the course of the transport process the quantity of the transported ACh^+ ions has gradually increased, showing that at the first 15 s of the transport process 0.29 μM of 100 μM and 0.86 μM of 0.1 M have been delivered across the membrane. At the end of the 20 min transport process, 0.0044% of 0.1 M and 2.77% of 100 μM initial concentrations have been delivered to the opposite side. Basically, these results show that the capacity of BPS transportability is dependent on the concentration of source solution, and the amount of crossover ACh^+ can vary even at extremely short transport durations. Moreover, fluorometric analyses have been used as successful characterization and quantification techniques, proving that both BPS ionomer and a highly simple and scalable ACh^+ Pen system can operate as a successful ACh^+ transporter.

Nonetheless, considering the future *in vivo* applicability of ACh^+ Pen, its main drawbacks, such as dimensional constraints and inadaptability to a tinier medium, have motivated us to develop a novel device design. The details of a more delicately projected architecture, miniaturized ACh^+ Pen, which is fabricated via a 3D-printer, are given in the Experimental Section and shown in Figure 3B-3. The essential difference that needs to be pointed out for the miniaturized ACh^+ Pen is the

https://dx.doi.org/10.1021/acsami.0c13725
ACS Appl. Mater. Interfaces XXXX, XXX, XXX−XXX

potential difference of 55 mV_{bias}, which has been applied during potentiostatic experiments. This value is the threshold depolarization potential that activates the action potential during the communication between neurons, and it has been applied to better approach the actual ACh^+ transport conditions. The reported performance data has been represented in both current (nA) and current density (nA cm^{-2}) forms (Figure S4B and Figure 3E). It can be observed from the inset of Figure 3E that the obtained potentiostatic performances through five sets of $J-t$ experiments, all conducted with a different miniaturized ACh^+ Pen, have generated comparable current densities. The inferences made from the generated current values (130−250 nA range) show that at even such miniaturized systems five sets of consecutive experiments revealed the performance values at close proximity, proving the factuality of the obtained results. The $J-t$ performances have been normalized to the cross-sectional area of the membrane, having a diameter of 5 mm, generating current densities in the 600−1200 nA cm^{-2} range.

Part 2: Setup of the Calibration Curve for Conductivity-Based Acetylcholine Sensor. During the ACh^+ detection steps, the requirement for enzyme-based quantification techniques, such as the fluorometric method, have been proven to be highly precise, yet time-consuming and expensive. In this regard, our research team has focused on developing an ionomer-based approach and, therefore for the very first time in the literature, has utilized ACh^+-BPS for the development of the conductivity-based, real-time sensor. The measurements have been conducted in a conductivity cell at the constant-temperature water bath. The initial steps of the analysis were based on the establishment of a calibration curve which has been achieved via equilibrating BPS for 24 h at different acetylcholine chloride solution concentrations ranging from 1 × 10^{-5} to 0.05 M. The obtained data set given in Figure S5 shows that during the primary immersion of the membrane into dilute acetylcholine chloride solutions a certain amount of time is required for the equilibration to occur. In other words, BPS reaches its steady-state conductivity value slower at low ACh^+ concentrations. On the other hand, the equilibration process speeds up at higher ACh^+ molarities. After the primary equilibration step was finished for the whole concentration range, the equilibrated membrane has been againward immersed into the same set of acetylcholine chloride solutions, consecutively. However, at this step, the conductivity values have only been evaluated at 1, 5, and 10 min to test the swiftness of the responsivity of membranes to changing concentrations. It has been observed from the obtained values that for an equilibrated membrane reaching a steady-state conductivity value within 1−10 min is possible. The impedance data obtained from the second equilibration test within the concentration range of 1 × 10^{-5}−0.05 M and their corresponding conductivity vs time column plots are specified in Figure S6. The given impedance plots, also termed Nyquist plots, have been fitted to the equivalent circuit shown in Figure 4, containing a resistance (R_1) being in series connection with parallel-connected "R_2-C_1" and "R_3-C_2". Here, R_1 stands for the resistance of ACh^+ electrolyte solution, while R_2 and C_1 are associated with the resistance and capacitance of BPS, respectively. On the other hand, R_3 and C_2 have been reported to represent the interfacial transport resistance and capacitances, respectively.[53] In accordance with previously reported studies that have analyzed membrane conductivities under different solution concentrations, herein, it can also be concluded that the membrane-related resistances are affected by the concentration of solution remaining in membrane domains.[53,54] Thus, the increasing ACh^+ concentration has been observed to have an ultimate impact on the membrane conductivities, which have been evaluated by using eq S1. Moreover, by combination of all the conductivity values obtained under the same analysis period at different concentrations, a linear relation can be established and can be used as a successful calibration curve (Figure S7). In general, these electrochemical preapplication characterizations have been fulfilled to develop a proper methodology for membrane equilibration, proving that the presence of a linear relationship between concentration and conductivity at extremely short periods like 1 min demonstrates the applicability of this system into a future ACh^+ quantitating sensor device.

Additionally, considering the transport of ACh^+ ions across the hydrophilic channels of BPS, the effect of reptation must also be considered. In one of the studies conducted by Onorato et al., the importance of polymeric structure, as well as the dissociation of ions, has been stated as a crucial parameter to be considered during the evaluation of ionic transport performance.[37] The study remarks that the transport via ionic hopping is directly related to the chain motion of polymers. This motion (i.e., reptation) increases because of increasing temperature, hence bringing to higher ionic transports at elevated temperatures. The given statement has been crosschecked for BPS where conductivity has been analyzed at the same solution concentration (0.05 M ACh^+) at both room temperature and 35 °C ambient conditions. It has been clearly observed from Figure S8 that the conductivity value significantly increases with the elevating solution temperature, showing the correlation between two parameters.

As a result, the ionic conductivities have been calculated by using the impedance of the BPS membrane and have been directly correlated to specific acetylcholine solution concentrations. In other words, conductivities ranging from 8 to 2000 mS cm^{-1} (Figure S7) represent the ACh^+ concentrations ranging from 1 × 10^{-5} to 0.05 M. However, to find an unknown concentration of ACh^+ in a solution, the setup must be re-formed into a tandem system design and collocated with the calibration curve, which is explained in detail in the following section.

Part 3: Conductivity-Based Acetylcholine Sensor and Development of Dual Transporter−Sensor System. The ultimate purpose of our study was to combine the self-developed ACh^+ delivery system with the conductivity-based sensor, hereby setting up a dual device that performs both operations concurrently. Thus, to find an unknown concentration of ACh^+ in a solution, the setup has been re-formed into a tandem system design and collocated with the calibration curve (Figure 4A). As it has already been established in the "Part 1" of the reported study, to provide the crossover of ACh^+ across the membrane, the opposite solution has been selected as conductive KCl. For the purposes of using dual transporter and sensor at the same time, the contents of the solutions for both operations had to be the same. That is why at this stage of the experiment BPS has been calibrated via impedance spectroscopy in solutions containing ACh^+ with concentrations changing within the 1 × 10^{-5}−0.05 M range and constantly present 100 nM KCl (Figure 4B and Figure S9). The obtained impedance plots have been fitted into the equivalent circuit (EC) given in Figure 4C. The

https://dx.doi.org/10.1021/acsami.0c13725
ACS Appl. Mater. Interfaces XXXX, XXX, XXX−XXX

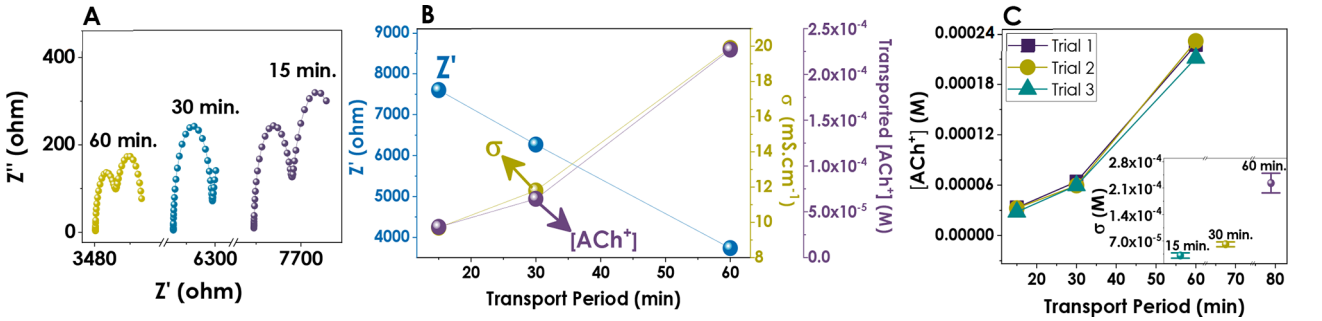

Figure 5. (A) Impedance plots obtained from solutions generated as a result of 15, 30, and 60 min of ACh^+ transport and the corresponding (B) BPS conductivities and evaluated unknown ACh^+ concentrations. (C) Repeatability testing of a tandem system with corresponding standard deviation statistics.

Table 1. Comparison of BPS-Based ACh^+ Biosensor with Other Nonenzymatic Biosensors Reported in the Literature

biosensor material	type of sensor	LoD	detection limit (μM)	ref
Ni−Al layered double hydroxide decorated with carbon nanoparticle	amperometric	0.005−6.88 mM	1.7	55
carbon paste electrode modified with Cu micro/nanoparticles	amperometric	0.12−2.68 mM	39	56
lichen-like NiO modified carbon paste	amperometric	0.25−5.88 mM	26.7	57
Ni nanowire	DC and AC amperometric		0.84 and 3.59	58
carbon electrode modified with magnetic core−shell structured manganese ferrite nanoparticles	voltammetric	0.1−500 μM	0.02	59
screen printed electrode modified with $ZnFe_2O_4$ nanoparticles	voltammetric	0.08−500 μM	0.024	60
carbon paste modified with graphene quantum dots/ionic liquid	voltammetric	0.2−400 μM	0.06	61
ACh^+-BPS/dual transporter and sensor	EIS based	10−50000 μM	33.4	this study

corresponding conductivities evaluated by using eq S1 have assisted in the establishment of the new calibration curves (Figure 4D). To test the effect of interference of K^+ cations, membranes' conductivities have been analyzed in three different solutions containing 0, 100, and 500 nM KCl, with 0.01 M ACh^+ being constantly present. The obtained results given in Figure S10A show that the interference of KCl at 100 nM is too small, affecting the conductivity values insignificantly. In contrast, the concentration of 500 nM increases the membrane conductivity, eventually interfering with the obtained results. Therefore, 100 nM KCl solution not only provides the necessary conductive ability to transport ACh^+ across the membrane but also generates a very tiny interference in conductivity measurements. Figures S10B−D have also been given to show that the presence of 100 nM KCl does not strongly disturb the linearity of the obtained calibration curve.

The tandem system has been operated as represented in Figure 4A and explained in detail in the Experimental Section. The transport of ACh^+ through BPS to the opposite compartment for 15, 30, and 60 min resulted in the establishment of Figure 5A, which gives the impedance plots of BPS evaluated at resulting solutions. By using eq S1, we converted the obtained impedance values into conductivities. In the homestretch of the experimental process, the insertion of the obtained conductivity values into the calibration curve (Figure 4D) eventuated in the detection of the amount of transported acetylcholine, which is marked as [ACh^+] in Figure 5B. Thus, concurrent operation of both BPS-based devices has been maintained by (i) conducting transport in a two-compartment concentration cell and (ii) analyzing the delivered solution via modified conductivity cell. It can be observed from the obtained [ACh^+] values that increasing transport durations resulted in a gradual increase in the amount of crossover ions where at the end of 60 min 227 μM of the 0.5 M initial ACh^+ concentration has been transported to the counter solution. The obtained results prove the operability of the dual system based on BPS, showing that a single membrane can act as both a selective transporter and a sensor simultaneously. To validate the accuracy of the system, three sets of transport each conducted with freshly prepared 0.5 M ACh^+ have been conducted for 15, 30, and 60 min. Figure 5C showing the ACh^+ concentrations obtained from three sets of transport-and-sensing experiments proves the consistency among the obtained outcomes. In addition, the inset of Figure 5C reports the standard deviation of the obtained amounts of transported ACh^+ showing a slight variation in the amounts of calculated concentration values, proving the reproducibility of the obtained outcomes.

The stability of the device to multiple cycles of both transport and sensing has been analyzed through consecutive test sets. Here, 15 min lasting ACh^+ transport tests have been repeated for 15 times, subjecting the transport device to operate for a continuous ∼4 h. Each transport set has been followed with the analyses of the opposite compartment's solution. Figure S11A reports the conductivities obtained from the 1st, 3rd, 5th, and 15th cycles showing an almost stable performance distribution of conductivity values throughout 4 h, with approximate values of transported ACh^+.

Additionally, ACh^+-BPS, being used as ACh^+ sensor in the conductivity cell, has been regenerated by consecutively retransforming the membrane into salt, proton, and ACh^+ forms, as explained in the Experimental Section. The obtained results given in Figure S11B show that, after being regenerated, ACh^+-BPS requires ∼24 h for equilibration to reach a constant value of conductivity. However, after being properly equilibrated, the measurability of the membrane does not change, sensing approximately the same value of conductivity from the solution obtained from 15 min lasting transport test.

https://dx.doi.org/10.1021/acsami.0c13725
ACS Appl. Mater. Interfaces XXXX, XXX, XXX−XXX

These two analyses have proven the long-term durability and regenerability of BPS membranes, consolidating them as strong candidates for membrane-based dual-transport-sensor devices. Moreover, it is noteworthy to say that the quantification of the amount of transported ACh^+ takes less than a minute, providing a fast measurement time as an additional advantage to this dual system.

Based on our elaborative researches, Table 1 has been established to compare the responses obtained from our BPS based sensor with other nonenzymatic ACh^+ biosensors reported in the literature so far. As can be seen from the given table, no studies on IEM-based ACh^+ biosensing have been encountered in the literature. Mostly, the conducted research focuses on metal- and metal oxide-based complex nanomaterials that require long preparation steps. Moreover, it is highly important to note that our study can be considered as one of the pioneering studies in the field of EIS-based nonenzymatic ACh^+ biosensors, which concurrently conducts transport and sensing.

3. CONCLUSIONS

In summary, for the very first time in the literature, BPS ionomers being formerly used in PEMFCs[32] have been implemented into dual ACh^+ transport-and-sensor system. The given tandem system, compared to the previously reported ones, possesses several important advantages, among which the transport under an actual action potential of 55 mV_{bias}, smartly constructed system design, biocompatible BPS ionomer that operates as both transporter and sensor, and almost instant quantification of ACh^+ are the most significant ones. In a large-scale analysis setup, the developed sensor has shown linearity within a 1×10^{-5}–0.05 M concentration range and the detection limit of 33.4 μM. The operability of this dual, self-developed, BPS-based, and nonenzymatic system proves that membranes are powerful tools possessing the strong potential for the development of future, neurotransmitter delivering, *in vivo* operating devices. We believe that this dual system possesses a futuristic approach toward the ongoing neurotransmitter transporter-and-sensor systems, which is going to turn into a strong, scientifically appealing subject, attracting lots of attention.

4. EXPERIMENTAL SECTION

4.1. Materials and Equipment. Acetylcholine chloride, potassium chloride (KCl), sulfuric acid (H_2SO_4), sodium hydroxide (NaOH), and dimethylacetamide (DMAc) used in membrane casting have been purchased from Sigma-Aldrich. The Fluorometric Acetylcholine Assay Kit containing all necessary chemicals required for the analysis has been purchased from Cell Biolabs. All of the chemicals have been used as received without any purification.

4.2. BPS Synthesis and Characterization. The synthesis methods and characterization of disulfonated poly(arylene ether sulfone) (BPS) have been previously reported elsewhere.[26,28,30] Having a 35 mol % of sulfonation degree, BPS possesses an IEC of 1.52 mequiv mg^{-1} and intrinsic viscosity (IV) of 1.2 g dL^{-1}. The IEC of BPS membrane has been obtained by immersing the acid form of the membrane in 50 mL of DI water containing 1 M sodium sulfate. The solution has been stirred overnight to allow the protons to exchange with sodium ions completely. In addition, the solution has been titrated with 0.01 M sodium hydroxide (NaOH) in which phenolphthalein was present as an indicator. IEC = $V_{NaOH}M_{NaOH}/W_{dry}$ has been used as the equation for the evaluation of the IEC value. Here, V_{NaOH} stands for the volume and M_{NaOH} stands for the concentration of NaOH used in titration. W_{dry} represents the dry weight of BPS. Intrinsic viscosity measurements have been performed in NMP containing 0.05 M lithium bromide, which was added to suppress the polyelectrolyte effect at 25 °C by using a Cannon-Ubbelohde viscometer. The molecular structure of the copolymer is specified in Figure S2A.

To transform copolymers into membrane form, BPS has been dissolved in DMAc and kept stirring overnight. Membrane solutions have been cast on clean glass substrates and dried under infrared lamps overnight to obtain their primary salt forms of BPS. On the proceeding step, acidification of membranes has been performed via boiling them in sulfuric acid (0.5 M) solution for 2 h and further continuing boiling in deionized water for an additional 2 h. As the final step, membranes have been acetylcholinated in the aqueous solution of ACh^+ (0.1 M) for 24 h and have been kept in DI water overnight to remove excess ACh^+ remaining on the BPS surface.

The IEC of the ACh^+-BPS membrane has been evaluated via acid–base titration of NaOH and H_2SO_4. A 18.1 mg sample of the ACh^+-BPS membrane has been added to a 0.01 M NaOH solution (10 mL) and heated on a steam bath for 1 h. Following the given step, the NaOH solution containing the ACh^+-BPS membrane has been titrated with 0.005 M H_2SO_4, generating an IEC value of 1.42.

Zetasizer measurements have been conducted via a SurPass 3 (Anton Paar). 10 mM KCl (pH 5.25) as an electrolyte flow solution has been used. Time-dependent zeta-potential measurements of ACh^+ and H^+ forms of BPS have been maintained for 17 min. The mean and standard deviation of the obtained zeta-potential values are reported in Figure S1.

4.3. Device Manufacturing. For the large-scale concentration cell experiments, a double-compartment cell (60 mL volume for each) has been filled with acetylcholine chloride (0.1 M) and KCl (0.1 M) and has been separated via ACh^+-BPS.

The ACh^+ Pen system consists of an ordinary pen filled with acetylcholine chloride solution containing an ACh^+-BPS attached to its tip. As the counter cell, a tiny vial containing KCl solution at the same volume with the inner acetylcholine chloride solution has been used. Two stainless steel plate electrodes inserted into acetylcholine chloride and KCl compartments have provided the potential difference between two compartments.

4.4. Performance Analyses. J–t measurements at constant 1 V_{bias} and 55 mV_{bias} have been performed on a Solartron 1260 and 1278A sourcemeter. The obtained current values have been divided by the active surface area of membranes (concentration cell: 8.6 cm^2; ACh^+ Pen: 0.28 cm^2) to obtain current density values.

4.5. AFM Analysis and Nano-FTIR. Atomic force microscopy analysis has been conducted to observe the differences in the hydrophilic domain dimensions after two different treatment steps. At soft tapping mode, prewetted membranes have been analyzed, and phase images have been captured via the Asylum MFP-3D device. The membranes have been hydrated before analysis to avoid the shrinking of the hydrophilic domains.

In-depth investigation of BPS membrane channels has been actualized via Nano-FTIR device consisting of a scattering scanning near-field optical microscope (i.e., s-SNOM) equipped with an AFM tip and an asymmetric interferometer for the acquisition of phase images and simultaneously conducting real-time IR spectroscopy. The AFM imaging has been conducted at tapping mode, and IR data collection has been performed in two separate beam channels, which comprise the (i) B: 840–1600 cm^{-1} and (ii) E: 1400–2100 cm^{-1} wavenumber ranges.

4.6. Fluorometric ACh^+ Detection. For the purposes of transport assertion, the detection of the amount of ACh^+ in the opposing compartment has been conducted by enzyme-based techniques, which reveal the presence of neurotransmitters via fluorescence characterization and quantifies it. ACh^+ Pen has been primarily implemented into a fluorometric ACh^+ assay kit, where the quantification of the ACh^+ ions transported across the membrane of ACh^+ Pen into phosphate buffer saline (PBS) containing dish under 1 V_{bias} has been conducted (Figure S12A). The working principle of the assay kit is based on a series enzymatic reactions, which are specified in Figure S12B. The four progressive reaction steps, including the interaction with acetylcholinesterase (AChE), choline oxidase

https://dx.doi.org/10.1021/acsami.0c13725
ACS Appl. Mater. Interfaces XXXX, XXX, XXX–XXX

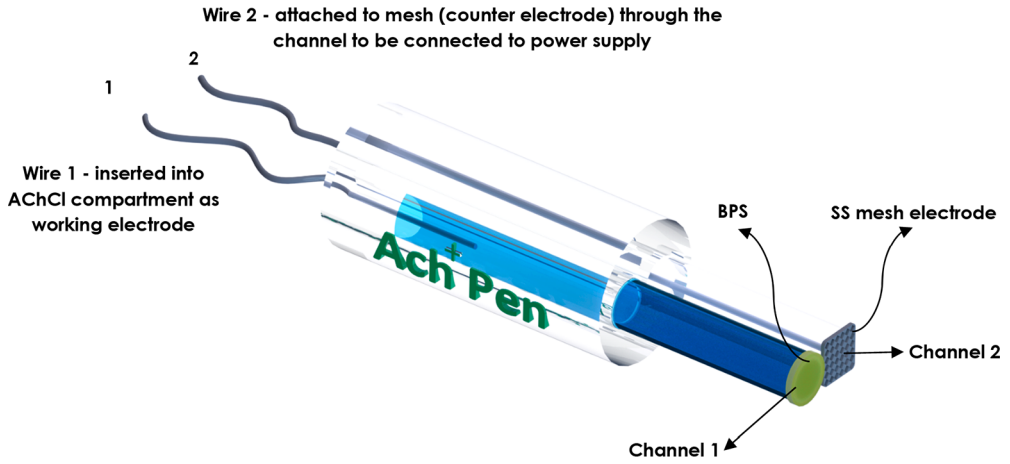

Figure 6. Miniaturized 3D-printed, self-designed ACh^+ Pen device consisting of two channels: (i) one serving as ACh^+ source with tiny BPS attached as selective transporter and (ii) the other consisting of SS-mesh serving as counter electrode for the counter solution.

(ChOx), and horseradish peroxidase (HRP) enzymes, result in the formation of hydrogen peroxide, which is designated via a fluorescence probe. HRP enzymes serve as the initiator of the catalysis reaction in-between the fluorescence probe and H_2O_2 (final product) and quantify the amount of ACh^+ which is formed in a 1:1 ratio. Two different initial concentration values of acetylcholine chloride solution (0.1 M and 100 μM) driven across the membrane in the ACh^+ Pen scale under 1 V bias have been analyzed. For each initial concentration, four sets of samples have been ejected from the opposing PBS solution at predetermined time intervals (t = 15, 60, 300, and 1200 s) and have been further diluted according to the procedure given in the assay kit.

4.7. Architecture of Miniaturized ACh^+ Pen. The miniaturized ACh^+ Pen is composed of two separate channels with each tip having a diameter of 5 mm and serving for membrane and stainless steel (SS) mesh fixation (Figure 6). In the executed system design, SS mesh stands for the counter electrode. A thin SS wire attached to the mesh from the inside of channel 2 provides the application potential, therefore generating a potential difference between the inner acetylcholine chloride solution and outer KCl. Another tiny SS wire is being positioned in the anodic channel containing the ACh^+ solution. In a similar manner, bias has been applied between two electrodes, resulting in the electronic-to-ionic transduction.

4.8. BPS Equilibration for ACh^+ Sensitivity Testing. During the equilibration step, the membrane-embedded in conductivity cell has been immersed in solutions (200 mL) of the different ACh^+ concentrations at 35 °C fixed temperature. The setup for conductivity measurements has been thoroughly planned to keep the bath temperature constant throughout the experiments. Conductivity data have been collected at 1, 3, and 24 h periods per each concentration value (Figure S5). This step has served for the detailed investigation of the change in membrane conductivity with time until the complete equilibration took place. It is important to mention that, prior to switching to a new analyzed concentration, membranes have been kept in a DI water bath at 35 °C for 2 h to remove the ACh^+ remaining on their surface. The conversion of the obtained impedance values to conductivities (mS cm^{-1}) has been done by using eq S1.

After finishing the primary equilibration step for the whole concentration range, we againward immersed the equilibrated membrane into the same set of acetylcholine chloride solutions, consecutively. However, at this step, the conductivity values have only been evaluated at 1, 5, and 10 min to test the swiftness of the responsivity of membranes to changing concentrations. It has been observed from the obtained values that for an equilibrated membrane reaching a steady-state conductivity value within 1−10 min is possible (Figure S6).

4.9. BPS Equilibration in 100 nM KCl for Tandem Testing of Dual ACh^+ Transporter−Sensor. At this step, ACh^+ transport has been conducted in large-scale concentration cells under 55 mV_{bias} and an initial ACh^+ concentration of 0.5 M. The opposite compartment, in this case, contained an extremely diluted KCl solution (100 nM), which has been specifically chosen to prevent the interference in the ACh^+ quantification step. Nevertheless, to prevent the interruption of KCl ions in counter solution, the established calibration curve has been over made by conducting the same set of conductivity experiments with varying concentrations of acetylcholine chloride from 1×10^{-5} to 0.05 M and a constant molarity of 100 nM KCl (Figure S9). The new calibration curve has been individually contrasted with those obtained from pristine ACh^+ in DI water and has been specified in Figures S10B−D. This way, the interference of 100 nM KCl in the quantification of ACh^+ concentration has been prevented. The set of samples prepared and analyzed in the dual system have been obtained by transporting ACh^+ from 0.5 M source solution across the membrane at different transport durations (15, 30, and 60 min). At the end of each set of experiments, the counter solution with 100 nM KCl and an unknown concentration of acetylcholine chloride has been withdrawn from the compartment to be immediately tested in a BPS-based ACh^+ sensor.

4.10. Regeneration of ACh^+-BPS. An ACh^+-BPS membrane has been inserted into 0.5 M NaOH solution for 2 h, followed by a boiling step in DI water for an additional 1 h to be transformed into the salt form. Being kept in DI water at room temperature overnight, salt-BPS has been protonated and acetylcholinated in a similar manner as explained in section 4.2. After the completion of the acetylcholination step, ACh^+-BPS has been inserted into the conductivity cell and tested in a solution obtained from 15 min lasting transport experiment. The obtained conductivity value from the given solution has gradually dropped within a 24 h period. In-between the conductivity measurement cycles, the membrane has been thoroughly washed in DI water to completely release the excess ACh^+ from the surface of BPS. At the end of 24 h, the obtained conductivity has reached an equilibrium generating 9.29 mS cm^{-1}, showing that BPS membranes can be easily regenerated and equilibrated in a short period of time.

■ ASSOCIATED CONTENT

Supporting Information

The Supporting Information is available free of charge at https://pubs.acs.org/doi/10.1021/acsami.0c13725.

All necessary supporting figures and the establishment of calibration curves for the development of the ionomer-based sensor (PDF)

https://dx.doi.org/10.1021/acsami.0c13725
ACS Appl. Mater. Interfaces XXXX, XXX, XXX−XXX

AUTHOR INFORMATION

Corresponding Authors

Mehmet Sankir − *Micro and Nanotechnology Graduate Program and Department of Materials Science and Nanotechnology Engineering, TOBB University of Economics and Technology, 06560 Ankara, Turkey;* orcid.org/0000-0003-2103-0439; Email: mehmetsankir@gmail.com

Nurdan Demirci Sankir − *Micro and Nanotechnology Graduate Program and Department of Materials Science and Nanotechnology Engineering, TOBB University of Economics and Technology, 06560 Ankara, Turkey*; Email: ndsankir@gmail.com

Authors

Nazrin Abdullayeva − *Micro and Nanotechnology Graduate Program, TOBB University of Economics and Technology, 06560 Ankara, Turkey*

Alihan Kumtepe − *Micro and Nanotechnology Graduate Program, TOBB University of Economics and Technology, 06560 Ankara, Turkey*

Cigdem Tuc Altaf − *Micro and Nanotechnology Graduate Program, TOBB University of Economics and Technology, 06560 Ankara, Turkey*

Hakan Seckin − *Neurosurgery Clinic, Medicana Bursa Hospital, 16110 Bursa, Turkey*

Complete contact information is available at: https://pubs.acs.org/10.1021/acsami.0c13725

Author Contributions

N.A. and A.K. performed the fabrication and characterization of samples. N.A. and C.T.A. contributed to the data analysis and preparation of the manuscript. H.S. and M.S. contributed to the ACh^+ Pen performance analyses. M.S. is the principal investigator of the study. N.D.S., M.S., and N.A. performed the data analysis and wrote the manuscript. All authors reviewed and commented on the manuscript at all stages.

Funding

This study was supported by The Scientific and Technological Research Council of Turkey (TUBITAK) under the research Grant 217M641.

Notes

The authors declare no competing financial interest.

ACKNOWLEDGMENTS

The authors thank Melike Kaya and Didem Ketenoğlu from the Turkish Accelerator and Radiation Laboratory (TARLA) for helping in Nano-FTIR analysis. We also express our thanks to Anton Paar, Particle Analysis and Surface Charge, Graz, Austria, for their support during Zetasizer measurements.

ABBREVIATIONS

ACh^+, acetylcholine ion
ACh^+-BPS, acetylcholinated BPS
ACh^+ Pen, acetylcholine Pen
AChE, acetylcholine esterase
AChCl, acetylcholine chloride
AFM, atomic force microscope
BPS, disulfonated poly(arylene ether sulfone)
ChOx, choline oxidase
DMAc, dimethylacetamide
EC, equivalent circuit
FTIR, fourier transform infrared spectroscopy
FWHM, full width at half-maximum
HRP, horseradish peroxidase
IEM, ion exchange membranes
IR, infrared
KCl, potassium chloride
NaOH, sodiıum hydroxide
OEIP, organic electronic ion pump
OMIEC, organic mixed ionic−electronic conductors
PEDOT:PSS, poly(3,4-ethyle-nedioxythiophene):poly-(styrenesulfone)
PEMFC, proton-exchange membrane fuel cell
PBS, phosphate buffer saline
s-SNOM, scattering scanning near-field optical microscope
SS, stainless steel
XPS, X-ray photoelectron spectroscopy

REFERENCES

(1) Hulbert, A. J. Life, Death and Membrane Bilayers. *J. Exp. Biol.* **2003**, *206* (14), 2303−2311.

(2) Lane, N.; Martin, W. F. The Origin of Membrane Bioenergetics. *Cell* **2012**, *151* (7), 1406−1416.

(3) Bennett, A. Membranes in Industry: Facilitating Reuse of Wastewater. *Filtr. Sep.* **2005**, *42* (8), 28−30.

(4) Koros, W. J.; Kratochvil, A.; Shu, S.; Husain, S. Energy and Environmental Issues and Impacts of Membranes in Industry. *Membr. Oper. Innov. Sep. Transform.* **2009**, 139−165.

(5) Wang, L.; Boutilier, M. S. H.; Kidambi, P. R.; Jang, D.; Hadjiconstantinou, N. G.; Karnik, R. Fundamental Transport Mechanisms, Fabrication and Potential Applications of Nanoporous Atomically Thin Membranes. *Nat. Nanotechnol.* **2017**, *12* (6), 509−522.

(6) Li, N. N.; Fane, A. G.; Ho, W. S. W.; Matsuura, T. *Advanced Membrane Technology and Applications*; 2008. DOI: 10.1002/9780470276280.

(7) Ghosh, R. In *Application of Membranes in Biotechnology*; Hoek, E. M. V., Tarabara, V. V., Eds.; John Wiley & Sons, Inc.: 2013.

(8) Green, J. J.; Elisseeff, J. H. Mimicking Biological Functionality with Polymers for Biomedical Applications. *Nature* **2016**, *540* (7633), 386−394.

(9) Hu, C. M. J.; Fang, R. H.; Wang, K. C.; Luk, B. T.; Thamphiwatana, S.; Dehaini, D.; Nguyen, P.; Angsantikul, P.; Wen, C. H.; Kroll, A. V.; Carpenter, C.; Ramesh, M.; Qu, V.; Patel, S. H.; Zhu, J.; Shi, W.; Hofman, F. M.; Chen, T. C.; Gao, W.; Zhang, K.; Chien, S.; Zhang, L. Nanoparticle Biointerfacing by Platelet Membrane Cloaking. *Nature* **2015**, *526* (7571), 118−121.

(10) Tybrandt, K.; Larsson, K. C.; Kurup, S.; Simon, D. T.; Kjäll, P.; Isaksson, J.; Sandberg, M.; Jager, E. W. H.; Richter-Dahlfors, A.; Berggren, M. Translating Electronic Currents to Precise Acetylcholine-Induced Neuronal Signaling Using an Organic Electrophoretic Delivery Device. *Adv. Mater.* **2009**, *21* (44), 4442−4446.

(11) Simon, D. T.; Kurup, S.; Larsson, K. C.; Hori, R.; Tybrandt, K.; Goiny, M.; Jager, E. W. H.; Berggren, M.; Canlon, B.; Richter-Dahlfors, A. Organic Electronics for Precise Delivery of Neurotransmitters to Modulate Mammalian Sensory Function. *Nat. Mater.* **2009**, *8* (9), 742−746.

(12) Xu, Y.; Yan, J.; Zhou, P.; Li, J.; Gao, H.; Xia, Y.; Wang, Q. Neurotransmitter Receptors and Cognitive Dysfunction in Alzheimer's Disease and Parkinson's Disease. *Prog. Neurobiol.* **2012**, *97* (1), 1−13.

(13) Poewe, W.; Seppi, K.; Tanner, C. M.; Halliday, G. M.; Brundin, P.; Volkmann, J.; Schrag, A. E.; Lang, A. E. Parkinson Disease. *Nat. Rev. Dis. Prim.* **2017**, *3*, 1−21.

(14) Xie, Z.-q.; Tian, X.-t.; Zheng, Y.-m.; Zhan, L.; Chen, X.-q.; Xin, X.-m.; Huang, C.-g.; Gao, Z.-b. Antiepileptic Geissoschizine Methyl Ether Is an Inhibitor of Multiple Neuronal Channels. *Acta Pharmacol. Sin.* **2020**, *41* (5), 629−637.

https://dx.doi.org/10.1021/acsami.0c13725
ACS Appl. Mater. Interfaces XXXX, XXX, XXX−XXX

(15) Picciotto, M. R.; Higley, M. J.; Mineur, Y. S. Acetylcholine as a Neuromodulator: Cholinergic Signaling Shapes Nervous System Function and Behavior. *Neuron* **2012**, *76* (1), 116−129.
(16) Schaaf, C. P. Nicotinic Acetylcholine Receptors in Human Genetic Disease. *Genet. Med.* **2014**, *16* (9), 649−656.
(17) Arbring Sjöström, T.; Berggren, M.; Gabrielsson, E. O.; Janson, P.; Poxson, D. J.; Seitanidou, M.; Simon, D. T. A Decade of Iontronic Delivery Devices. *Adv. Mater. Technol.* **2018**, *3* (5), 1−10.
(18) Paulsen, B. D.; Tybrandt, K.; Stavrinidou, E.; Rivnay, J. Organic Mixed Ionic−Electronic Conductors. *Nat. Mater.* **2020**, *19* (1), 13−26.
(19) Isaksson, J.; Nilsson, D.; Kjäll, P.; Robinson, N. D.; Richter-Dahlfors, A.; Berggren, M. Electronically Controlled PH Gradients and Proton Oscillations. *Org. Electron.* **2008**, *9* (3), 303−309.
(20) Abdullayeva, N.; Sankir, M. Influence of Electrical and Ionic Conductivities of Organic Electronic Ion Pump on Acetylcholine Exchange Performance. *Materials* **2017**, *10* (6), 1−13.
(21) Isaksson, J.; Kjäll, P.; Nilsson, D.; Robinson, N.; Berggren, M.; Richter-Dahlfors, A. Electronic Control of Ca2+ Signalling in Neuronal Cells Using an Organic Electronic Ion Pump. *Nat. Mater.* **2007**, *6* (9), 673−679.
(22) Poxson, D. J.; Karady, M.; Gabrielsson, R.; Alkattan, A. Y.; Gustavsson, A.; Doyle, S. M.; Robert, S.; Ljung, K.; Grebe, M.; Simon, D. T.; Berggren, M. Regulating Plant Physiology with Organic Electronics. *Proc. Natl. Acad. Sci. U. S. A.* **2017**, *114* (18), 4597−4602.
(23) Seitanidou, M.; Franco-Gonzalez, J. F.; Sjöström, T. A.; Zozoulenko, I.; Berggren, M.; Simon, D. T. PH Dependence of γ-Aminobutyric Acid Iontronic Transport. *J. Phys. Chem. B* **2017**, *121* (30), 7284−7289.
(24) Semiz, L.; Sankir, N. D.; Sankir, M. Directly Copolymerized Disulfonated Poly(Arylene Ether Sulfone) Membranes for Vanadium Redox Flow Batteries. *Int. J. Electrochem. Sci.* **2014**, *9* (6), 3060−3067.
(25) Semiz, L.; Demirci Sankir, N.; Sankir, M. Influence of the Basic Membrane Properties of the Disulfonated Poly(Arylene Ether Sulfone) Copolymer Membranes on the Vanadium Redox Flow Battery Performance. *J. Membr. Sci.* **2014**, *468*, 209−215.
(26) Kim, Y. S.; Einsla, B.; Sankir, M.; Harrison, W.; Pivovar, B. S. Structure-Property-Performance Relationships of Sulfonated Poly(Arylene Ether Sulfone)s as a Polymer Electrolyte for Fuel Cell Applications. *Polymer* **2006**, *47* (11), 4026−4035.
(27) Zhang, Z. B.; Fan, G. Y.; Sankir, M.; Park, H. B.; Freeman, B. D.; McGrath, J. E. Synthesis of Di-Sulfonated Poly (Arylene Ether Sulfone) Random Copolymer as Novel Candidates for Chlorine-Tolerant Reverse Osmosis Membranes. *ACS PMSE Prepr.* **2006**, *95*, 887−888.
(28) Sankir, M.; Bhanu, V. A.; Harrison, W. L.; Ghassemi, H.; Wiles, K. B.; Glass, T. E.; Brink, A. E.; Brink, M. H.; McGrath, J. E. Synthesis and Characterization of 3,3 - Disulfonated 4,4- Dichlorodiphenyl Sulfone (SDCDPS) Monomer for Proton Exchange Membranes (PEM) in Fuel Cell Applications. *J. Appl. Polym. Sci.* **2006**, *100*, 4595−4602.
(29) Sankir, M.; Bhanu, V. A.; Harrison, W. L.; Ghassemi, H.; Wiles, K. B.; Glass, T. E.; Brink, A. E.; Brink, M. H.; McGrath, J. E. Synthesis and Characterization of 3,3′-Disulfonated-4,4′- Dichlorodiphenyl Sulfone (SDCDPS) Monomer for Proton Exchange Membranes (PEM) in Fuel Cell Applications. *J. Appl. Polym. Sci.* **2006**, *100* (6), 4595−4602.
(30) Park, H. B.; Freeman, B. D.; Zhang, Z. B.; Sankir, M.; McGrath, J. E. Highly Chlorine-Tolerant Polymers for Desalination. *Angew. Chem., Int. Ed.* **2008**, *47* (32), 6019−6024.
(31) Wang, T.; Li, T.; Aboki, J.; Guo, R. Disulfonated Poly(Arylene Ether Sulfone) Random Copolymers Containing Hierarchical Iptycene Units for Proton Exchange Membranes. *Front. Chem.* **2020**, *8*, 1−12.
(32) Sankir, M.; Semiz, L.; Sankir, N. D. Catalyst Free Hydrogen Generation from Directly Disulfonated Poly(Arylene Ether Sulfone) Copolymer Membranes. *J. Membr. Sci.* **2015**, *496*, 318−324.
(33) Moon, J. M.; Thapliyal, N.; Hussain, K. K.; Goyal, R. N.; Shim, Y. B. Conducting Polymer-Based Electrochemical Biosensors for Neurotransmitters: A Review. *Biosens. Bioelectron.* **2018**, *102*, 540−552.
(34) Sinha, R.; Ganesana, M.; Andreescu, S.; Stanciu, L. AChE Biosensor Based on Zinc Oxide Sol-Gel for the Detection of Pesticides. *Anal. Chim. Acta* **2010**, *661* (2), 195−199.
(35) Chauhan, N.; Chawla, S.; Pundir, C. S.; Jain, U. An Electrochemical Sensor for Detection of Neurotransmitter-Acetylcholine Using Metal Nanoparticles, 2D Material and Conducting Polymer Modified Electrode. *Biosens. Bioelectron.* **2017**, *89*, 377−383.
(36) Walsh, R.; Morales, J. M.; Skipwith, C. G.; Ruckh, T. T.; Clark, H. A. Enzyme-Linked DNA Dendrimer Nanosensors for Acetylcholine. *Sci. Rep.* **2015**, *5*, 1−11.
(37) Onorato, J. W.; Luscombe, C. K. Morphological Effects on Polymeric Mixed Ionic/Electronic Conductors. *Mol. Syst. Des. Eng.* **2019**, *4* (2), 310−324.
(38) Xue, Z.; He, D.; Xie, X. Poly(Ethylene Oxide)-Based Electrolytes for Lithium-Ion Batteries. *J. Mater. Chem. A* **2015**, *3* (38), 19218−19253.
(39) Padma Kumar, P.; Yashonath, S. Ionic Conduction in the Solid State. *Proc. Indian Acad. Sci.* **2006**, *37* (24), 135−154.
(40) Shah, D. B.; Olson, K. R.; Karny, A.; Mecham, S. J.; DeSimone, J. M.; Balsara, N. P. Effect of Anion Size on Conductivity and Transference Number of Perfluoroether Electrolytes with Lithium Salts. *J. Electrochem. Soc.* **2017**, *164* (14), A3511−A3517.
(41) Huth, F.; Govyadinov, A.; Amarie, S.; Nuansing, W.; Keilmann, F.; Hillenbrand, R. Nano-FTIR Absorption Spectroscopy of Molecular Fingerprints at 20 Nm Spatial Resolution. *Nano Lett.* **2012**, *12* (8), 3973−3978.
(42) Wang, F.; Hickner, M.; Kim, Y. S.; Zawodzinski, T. A.; McGrath, J. E. Direct Polymerization of Sulfonated Poly(Arylene Ether Sulfone) Random (Statistical) Copolymers: Candidates for New Proton Exchange Membranes. *J. Membr. Sci.* **2002**, *197*, 231−242.
(43) Kim, Y. S.; Hickner, M. A.; Dong, L.; Pivovar, B. S.; McGrath, J. E. Sulfonated Poly(Arylene Ether Sulfone) Copolymer Proton Exchange Membranes: Composition and Morphology Effects on the Methanol Permeability. *J. Membr. Sci.* **2004**, *243* (1−2), 317−326.
(44) Sankir, M.; Kim, Y. S.; Pivovar, B. S.; McGrath, J. E. Proton Exchange Membrane for DMFC and H2/Air Fuel Cells: Synthesis and Characterization of Partially Fluorinated Disulfonated Poly(Arylene Ether Benzonitrile) Copolymers. *J. Membr. Sci.* **2007**, *299* (1−2), 8−18.
(45) Oh, K. H.; Bae, I. Engineered Membrane-Electrode Interface for Hydrocarbon-Based Polymer-Electrolyte-Membrane Fuel Cells via Solvent-Vapor-Annealed Deposition. *ACS Appl. Nano Mater.* **2019**, *2* (6), 3857−3863.
(46) Epsztein, R.; DuChanois, R. M.; Ritt, C. L.; Noy, A.; Elimelech, M. Towards Single-Species Selectivity of Membranes with Sub-nanometre Pores. *Nat. Nanotechnol.* **2020**, *15*, 426−436.
(47) MacKsasitorn, S.; Changkhamchom, S.; Sirivat, A.; Siemanond, K. Sulfonated Poly(Ether Ether Ketone) and Sulfonated Poly(1,4-Phenylene Ether Ether Sulfone) Membranes for Vanadium Redox Flow Batteries. *High Perform. Polym.* **2012**, *24* (7), 603−608.
(48) Mauritz, K. A.; Moore, R. B. State of Understanding of Nafion. *Chem. Rev.* **2004**, *104* (10), 4535−4585.
(49) Kunimatsu, K.; Yagi, K.; Bae, B.; Miyatake, K.; Uchida, H.; Watanabe, M. ATR-FTIR Analysis of the State of Water in a Sulfonated Block Poly(Arylene Ether Sulfone Ketone) Membrane and Proton Conductivity Measurement during the Hydration/Dehydration Cycle. *J. Phys. Chem. C* **2013**, *117* (8), 3762−3771.
(50) Taucher, T. C.; Hehn, I.; Hofmann, O. T.; Zharnikov, M.; Zojer, E. Understanding Chemical versus Electrostatic Shifts in X-Ray Photoelectron Spectra of Organic Self-Assembled Monolayers. *J. Phys. Chem. C* **2016**, *120* (6), 3428−3437.
(51) Tardio, S.; Cumpson, P. J. Practical Estimation of XPS Binding Energies Using Widely Available Quantum Chemistry Software. *Surf. Interface Anal.* **2018**, *50* (1), 5−12.
(52) Jeyavijayan, S. Spectroscopic (FTIR, FT-Raman), Molecular Electrostatic Potential, NBO and HOMO-LUMO Analysis of P-

https://dx.doi.org/10.1021/acsami.0c13725
ACS Appl. Mater. Interfaces XXXX, XXX, XXX−XXX

Bromobenzene Sulfonyl Chloride Based on DFT Calculations. *Spectrochim. Acta, Part A* **2015**, *136* (PB), 890−899.
(53) Fontananova, E.; Zhang, W.; Nicotera, I.; Simari, C.; van Baak, W.; Di Profio, G.; Curcio, E.; Drioli, E. Probing Membrane and Interface Properties in Concentrated Electrolyte Solutions. *J. Membr. Sci.* **2014**, *459*, 177−189.
(54) Huang, Q.; Luo, Q.; Chen, Z.; Yao, L.; Fu, P.; Lin, Z. The Effect of Electrolyte Concentration on Electrochemical Impedance for Evaluating Polysulfone Membranes. *Environ. Sci. Water Res. Technol.* **2018**, *4* (8), 1145−1151.
(55) Wang, L.; Chen, X.; Liu, C.; Yang, W. Non-Enzymatic Acetylcholine Electrochemical Biosensor Based on Flower-like NiAl Layered Double Hydroxides Decorated with Carbon Dots. *Sens. Actuators, B* **2016**, *233*, 199−205.
(56) Heli, H.; Hajjizadeh, M.; Jabbari, A.; Moosavi-Movahedi, A. A. Copper Nanoparticles-Modified Carbon Paste Transducer as a Biosensor for Determination of Acetylcholine. *Biosens. Bioelectron.* **2009**, *24* (8), 2328−2333.
(57) Sattarahmady, N.; Heli, H.; Vais, R. D. An Electrochemical Acetylcholine Sensor Based on Lichen-like Nickel Oxide Nanostructure. *Biosens. Bioelectron.* **2013**, *48*, 197−202.
(58) Blanco, S.; Vargas, R.; Mostany, J.; Borrás, C.; Scharifker, B. R. A Novel Nickel Nanowire Amperometric Sensor: Direct Current vs. Alternating Current Strategies for Ethanol, Acetaldehyde and Acetylcholine Detection. *J. Electroanal. Chem.* **2015**, *740*, 61−67.
(59) Mohammadi, S. Z.; Beitollahi, H.; Tajik, S. Nonenzymatic Coated Screen - Printed Electrode for Electrochemical Determination of Acetylcholine. *Micro Nano Syst. Lett.* **2018**, *6*, 1−7.
(60) Beitollahi, H.; Safaei, M.; Tajik, S. Screen-Printed Electrode Modified with ZnFe2O4 Nanoparticles for Detection of Acetylcholine. *Electroanalysis* **2019**, *31* (6), 1135−1140.
(61) Jahani, P. M.; Jafari, M.; Gupta, V. K.; Agarwal, S. Graphene Quantum Dots/Ionic Liquid-Modified Carbon Paste Electrode-Based Sensor for Simultaneous Voltammetric Determination of Norepinephrine and Acetylcholine. *Int. J. Electrochem. Sci.* **2020**, *15* (1), 947−958.

https://dx.doi.org/10.1021/acsami.0c13725
ACS Appl. Mater. Interfaces XXXX, XXX, XXX−XXX